

Stick-slip Avalanches in Steady Shearing: Signature of Transition between Granular Fluid and Solid

Jih-Chiang (JC) Tsai ^{1*}, Guan-Hao Huang ¹, and Cheng-En Tsai ^{1,2}

¹ Institute of Physics, Academia Sinica, Taipei, Taiwan

² Department of Physics, Nat'l Central University, Chung-Li, Taiwan

Correspondence (*): jctsai@phys.sinica.edu.tw

Abstract -- By observing the fluctuations of fluid-immersed granular particles upon steady shearing, we identify a transitional zone that sets the system apart from fluidic sliding and signals the onset of solid mechanics, as the shear rate decreases. Toward the slow extreme, statistical analyses of the avalanche events combined with internal imaging capture the continuous yet distinctive change of behaviors, and offer test grounds for theories on the development of plasticity. We link such transition with the velocity weakening of inter-particle frictions, and propose a three-state phase diagram that bridges our discoveries on tightly packed granular systems and previous understanding of suspension rheology.

Granular-fluid systems are excellent examples exhibiting solid-fluid duality. In the past decade, paradigms have been established for understanding the rheology of granular suspensions [1] where fluid-mediated particle interactions warrant a smooth flow at low shear rates. At densities well above the jamming point, the same system can instead withstand a shear stress indefinitely, behaving like a solid. The macroscopic deformation of granular solid often rely on different traditions such as elastoplastic modelling [2] to describe. Understanding the transition between these two extreme remains profound challenges, not only in the sophistication of theories treating partial fluidizations [3–5], but also due to the lack of experimental observation along such transition [6]. As a quasi-static problem, one recent consensus since the initial proposal of the jamming phase diagram [7] has been that the jamming point depends on inter-particle friction [8], and it is friction that makes a granular packing go beyond “ideal jamming” and exhibit fragile states where imposed shearing plays decisive roles [9–12]. Growing pieces of evidence have shown that tangential force between particles can also lead to dramatic changes in dynamics of rapid flows: Examples include experiments [13–15] or simulations [16,17], as a result of either actively turning on the friction, or of increasing the collisional stress above a critical load such that abrupt shear-thickening would occur.

For a tightly-packed system exhibiting long-lasting inter-particle contacts, most notably in geophysics, velocity-dependent frictions are often considered the root of instabilities leading to catastrophic consequences like earthquakes [18–20] or hysteresis in laboratory studies [21]. Most existing work, however, do not address how the velocity dependence of friction between single grains could affect the flow at the macroscopic level. Nevertheless, one recent work reports the correlation between the mean flow of sheared emulsion and the tribology of constituent particles [22].

In this Letter, we demonstrate that high packing fraction is just a necessary condition for creating solid-like response. The imposed shear rate plays a crucial role on the regime transition. We identify a transitional zone that is intimately connected to the velocity-dependent friction at the grain level. Along the transition, prominent stick-slip avalanches provide an unambiguous sign setting apart viscous sliding (like a fluid) and plastic yielding (like a solid). Based on our observations, we propose a three-state diagram that integrate the flows of interlocked solid, lubricated sliders, and suspended granular particles on one single landscape controlled by the shear rate and the confining volume (or pressure).

Setup and overview of transitions --- Shown as in Fig.1(a), our particles fill the space between two cones. The sidewall is formed by a stack of free-sliding acrylic rings with an inner diameter $2R=22\text{cm}$. Two cones are geometrically roughed at the scale of the particle with diameter $d\approx 9\text{mm}$. The upper cone is set at a fixed height, with the mechanism specially reinforced to provide a smooth rotation at an angular resolution of $2\pi\cdot 10^{-4}$ with a wide range of angular speeds Ω . The base of the system is supported by the arrangement of six independent force sensors, in order to determine the total forces and moments that keep the base stationary. The gap between the rotating boundary and the sidewall is 2mm such that all particles cannot escape. The nominal volume fraction is defined as $\phi = N v_1 / V_{\text{access}}$ in which $N=O(1000)$ is the number of particles. V_{access} represents the total volume accessible by the particles, and v_1 stands for the volume for the single particle (which has been determined by Archimede's method and checked for the mono-dispersity). Simultaneously, we take internal images of particles through the bottom, when the interstitial space is filled with aqueous solution of 60% glycerol such that the refraction index is matched to the particles [23,24]. We illuminate the system at its mid-height, with a horizontal laser sheet at the wavelength of 532nm going through the 1mm gap between the tips of two cones. Image contrasts are generated by dyeing either particles or the fluid with Rhodamine. Data reported in this paper are based on spherical particles of polydimethylsiloxane (PDMS) elastomer that we create by molding: We use the default 10:1 ratio with crosslinking agent [25] ; the particles exhibit a Hertzian response to compression with a Young's modulus around 1.5MPa [33].

Figure 1(b) presents an overview of transitions, by showing the statistical distributions of instantaneous torque (presented as an effective stress in kPa). Data include experiments using different rotation rates ranging from 0.05 to 0.0001 rev/s (rps), all at the same $\phi=0.60$. At either the fast or the slow end, the histogram exhibits a bell shape on the semi-log plot close to a parabola. Note that the slower runs are at the state of *higher* stress, in startling contrast with reported studies on most rheometric flows [26–28]. Interestingly, between the two extremes, the data show series of transitional states with histograms that are highly asymmetrical. We label the case at 0.005rps as state-T. The strong asymmetry can be understood by observing the time series of torque --- see Fig.1(c). It shows that state-T exhibits abrupt changes of torque, with several large drops per unit *strain* ($\equiv \Delta\theta / 2\tan \xi$, see Fig.1a), and the concavity of the curve connecting the drops provides a minimal explanation of the asymmetry. We also label the other representative high-stress (low-stress) state as state- $\beta(\alpha-)$, for the convenience of subsequent discussions.

In analogy to conventional rheology, we define “flow curves” by time-averaging the effective stress σ_S and plot them against the shear rate $\dot{\gamma}$ ($\equiv \Omega/2 \tan \xi$) ---see Fig.1(d). This includes data from experiments at a wider range of rotation rates than that in Fig.1(b), plus two additional experiments using fluids at higher viscosities (by adjusting the concentration of glycerol). The trend shows not only an interval of $\dot{\gamma}$ with negative slope, but also a minimum with an uprising of stress at higher shear rates. For all experiments up to 0.05rps, we also compute the normalized occurrence of the large drops (LD, defined as drops of torque that are larger than twice the root-mean-square of the total fluctuation --- see Supplements[33]) as a simple indicator to characterize the stick-slip fluctuations. We also incorporate the measurement of normal stress $\sigma_N \equiv$ time-averaged $F_z/\pi R^2$ and plot the counts of LD per unit strain against the viscous number $J \equiv \eta \dot{\gamma}/\sigma_N$ [1] as Fig.1(e). The data show a consistent rise and fall over the change of J , and reassure that the state we label as α - (at 0.05rps) belongs to the falling branch of the trend.

Approaching the plastic regime --- We find the gradual change from state-T to state- β deserves special attention. Fig.2(a) shows the cumulative distributions of drop events in torque: At each driving rate, we count the number of drops with the magnitude larger than a variable threshold Δ_{min} . The event counts are normalized by the total strain, and are plotted against Δ_{min} normalized by the mean torque at each driving rate. The change is striking: At state-T, the statistics indicates that for an accumulation of strain close to unity, one can expect at least one drop with a magnitude over 40% of the mean. In contrast, at state- β , such probability is two-decade smaller: a comparable drop becomes *extremely rare* such that it takes a strain $\sim O(100)$ to get one. The inset graph shows the log-log plot for three long runs. At state-T, the statistics exhibits a dramatic change in the logarithmic slope as $\Delta_{min}/\langle torque \rangle$ approaches unity, showing the effect of a characteristic scale set by the mean stress. In contrast, state- β presents a scale-free behavior with a constant slope (between -2.5 and -3) that spans over two decades in probabilities, because rearrangements are mostly *localized* such that the associated stress releases are never comparable to the mean --- We show in Fig.2(e) that all detected particle movements are highly isolated, often within the range of one single particle or just a few. This is in startling contrast with state-T, for which we show in Fig.2(d) the system-wise landslides that are in-sync with large drops of torque.

The dramatic difference between state-T and state- β are further illustrated by the scattered plots of the multi-component force data (Fig.2b-c), At state-T, the *torque*- F_z plot in Fig.2(b) reveals multiple traces of “loading” processes

between abrupt drops. By observing the time series of *torque* and F_z (not shown), we note that the growth of F_z with the angular displacement during the loading processes is closer to linear than that of *torque*; this explains the concavity of those traces on the *torque*- F_z plane. Meanwhile, the F_y - F_x plot can be regarded as a reduced phase space and reveals multiple *clusters* corresponding to processes of loading, as well as sudden “jumps” in-between that interrupt the stress build-up. For state-T, such jumps “reset” the system at the frequency of several times per unit strain. On the contrary, for state- β , such resets are rare. As a result, the system is kept at a higher level of mean stress than that of state-T, with fluctuations being infinitesimally small.

Connection with tribology and a three-state diagram – The intriguing rate-dependent transitions can be understood by considering two facts. (1) Illustrated as Fig.3(a), imposing a shear rate $\dot{\gamma}$ to a densely packed system creates a range of relative speeds among particles. In a system that is strongly damped, the anticipated distribution should be around the most probable speed $\sim d \dot{\gamma}$. (2) By independent measurements using the same fluid and PDMS elastomer with a radius of curvature $R=d/2$ to mimic our main experiments, we characterize the speed-dependent friction between surfaces – see Fig.3(b). The results show a characteristic speed V_c beyond which the tangential force decreases dramatically. Such effects are consistent with the transition from the regime of solid-solid friction to that of mixed lubrication, that is commonly cited as part of the Stribeck diagram in tribology involving fluids [14,30]. We have also confirmed that V_c is inversely proportional to the fluid viscosity, in consistence with prior literatures.

Figure 3(c) combines results from datasets from our main experiments with different volume fractions and fluid viscosities, and an interesting picture emerges on the two-parameter landscape mimicking the “three states of matter”. For each dataset, we plot the time-averaged shear stress σ_S as its vertical coordinate, against the mean normal stress σ_N and the dimensionless shear rate $d \dot{\gamma} / V_c$. The choice of these volume fractions warrants that σ_N are high enough to override the effect of gravity (due to about 10% mismatch of density) with ϕ going above the upper limit in most stress-controlled shear-flow experiments (~ 0.58 , such as in Ref. [31]). Note the negative slopes of σ_S over the shear rate, accompanied by the occurrence of stick-slips (highlighted by the shaded area on the horizontal plane), provides an unambiguous signature separating the state of viscous sliding (state- α) and that of plastic yielding (state- β) at high volume fractions.

Such transition can be rationalized by comparing $d\dot{\gamma}$ to V_c . For $d\dot{\gamma}/V_c \gtrsim 1$, most contacts are in the status of low-friction and are expected to slide smoothly --- except that at much higher driving rates the system might jam again due to shear-thickening effects [13–17,27,28] that are beyond the current scope of discussion. However, at moderate shear rates with $d\dot{\gamma}/V_c$ smaller but close to unity, one would expect that a small but substantial fraction of contacts are sliding: As the shearing keeps changing the particle configuration, these sliding contacts gather by chance and create slip planes such that system-wise landslides occur. Lastly, in the slow extreme where $d\dot{\gamma}/V_c \ll 1$, all contacts are in a high-friction state such that particles are interlocked. Since cooperative sliding becomes probabilistically impossible, the only mechanism for the global rearrangement is the accumulation of localized yielding, i.e., the system responds to the macroscopic shearing with numerous isolated slips (Fig.2e) and is kept at a plateau of high stress (recalling Fig.1b,c) on the landscape.

Understandably, as the volume fraction decreases, the shaded area as well as the plateau are supposed to vanish such that the separation between state- α and state- β eventually vanishes, as “yield stress” (and stick-slips) cannot possibly exist when the system becomes a *suspension*. (We have verified by using precisely density-matched particles and fluid that this indeed occurs at ϕ below 0.48.) To connect with prior studies, we indicate several contours of J from 10^{-4} down to 10^{-9} on the horizontal plane. Our studies demonstrate how “granular solids” are formed as we reduce J by several orders of magnitude than reported values. (Most prior studies on granular suspensions are limited to $J > 10^{-5}$, as reviewed in Ref.[1]). We are aware of one recent work with a rotating drum [21] which reports that smooth flows cease to exist and hysteric avalanches occur, as J goes below a critical value $J_c \sim 10^{-6}$. In our experiments, we find that stick-slips are indeed the most prominent with J between 10^{-6} and 10^{-7} (recall Fig.1e). But our fixed-volume shearing provides a further extension, showing that avalanches can vanish again at the slow extreme (with $J \sim 10^{-9}$).

Summary and outlooks--- We design an experiment to clarify the relationship among three regimes of granular dynamics in one setup: suspension flows, lubricated sliding, and plastic yielding. We identify an unambiguous solid-fluid transition which can be understood as the competition between the shear rate $\dot{\gamma}$ and the velocity-weakening threshold V_c for densely packed particle pairs: (1) We show a “dangerous zone” of shear rates where the typical speeds between particles $d\dot{\gamma}$ lie slightly below V_c . In these cases, although the majority of contacts are in solid-solid friction that favors the build-up of shear stress, a small but non-negligible fraction of low-friction sliders can create system-wise avalanches that bring the system to a state of lower stress, in a frequency of several events per unit strain. We show direct visual evidence with the images of internal “landslides”, which are well in-sync with the stick-slip patterns in torque. (2) At sufficiently high shear rate when viscous lubrication overrides the solid-solid friction, *smooth sliding* generally occurs and can be seen as a continuation from the well-established *dense suspension* regime where the stress arises mainly from collisions [1]. (3) Upon reducing the shear rate, we demonstrate the evolution toward *plastic yielding* --- The system-wise “brittle” failures are gradually replaced with isolated slips, with corresponding stress drops becoming infinitesimally small. The change of event statistics provides direct tests to theories in understanding the “flow” of granular solids, such as whether incrementally reducing the concentration of sliders [32] would reproduce the evolution of avalanches we observe.

We stress that taking the velocity dependence of friction into account should be essential for making realistic predictions on the flow of granular solids, such as in geophysical contexts. For fundamental researches, this also leads to many open questions, such as whether the coupling between particle velocity distribution and the speed-dependent tribology might result in a milder jamming so that a “critical” density is no longer detectable, and whether the occurrence of avalanches can be modeled by generalizing theories based on the percolation of contacts [10], or by imposing a distribution of frictional coefficients in quasi-static simulations [12].

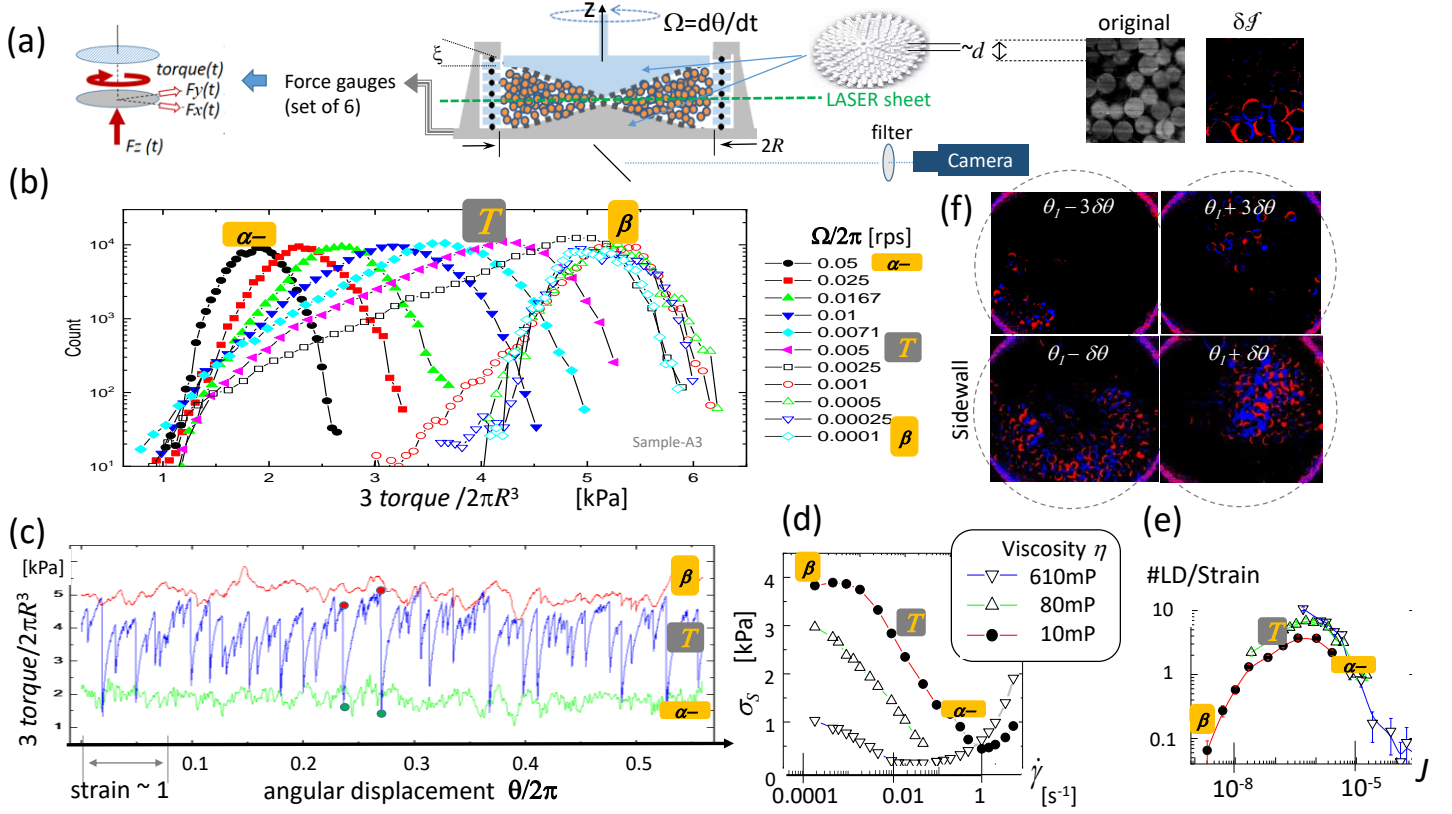


FIG. 1 (a) Schematics for the setup and measurements, from left to right: the time-dependent torque and three net forces as determined from sensors around the base; cross-sectional view of the main setup; 3D illustration of the roughened cones; close-up of one original fluorescent image; and the differential image $\delta\mathcal{I}$ computed from two frames with $\delta\theta = 8\pi \cdot 10^{-4}$. Pixels in positive (negative) values are displayed in blue (red). (b) Statistical distributions of measured torque, in steady states at different rotation rates $\Omega/2\pi$ (in revolution per second, rps). $\phi = 0.60$. (c) The time series of torque for three examples in (b), all plotted against the angular displacement. The high-frequency noise has been filtered with a cut-off at 40ms. (d) Time-averaged stress, plotted against the shear rate $\dot{\gamma}$. (e) Counts of LD (defined in main text) per unit strain, plotted against the viscous number J . Both (d) and (e) include data with fluids at three different viscosities. $\phi = 0.56$. (f) Sequence of $\delta\mathcal{I}$ with $\delta\theta = 2\pi \cdot 10^{-4}$, featuring one typical avalanche in state-T. The angular movement $\theta(t)$ are indicated in reference to a fixed θ_1 . These images are vivid demonstrations of dynamical heterogeneities [29] for systems near jamming, with videos provided online[33].

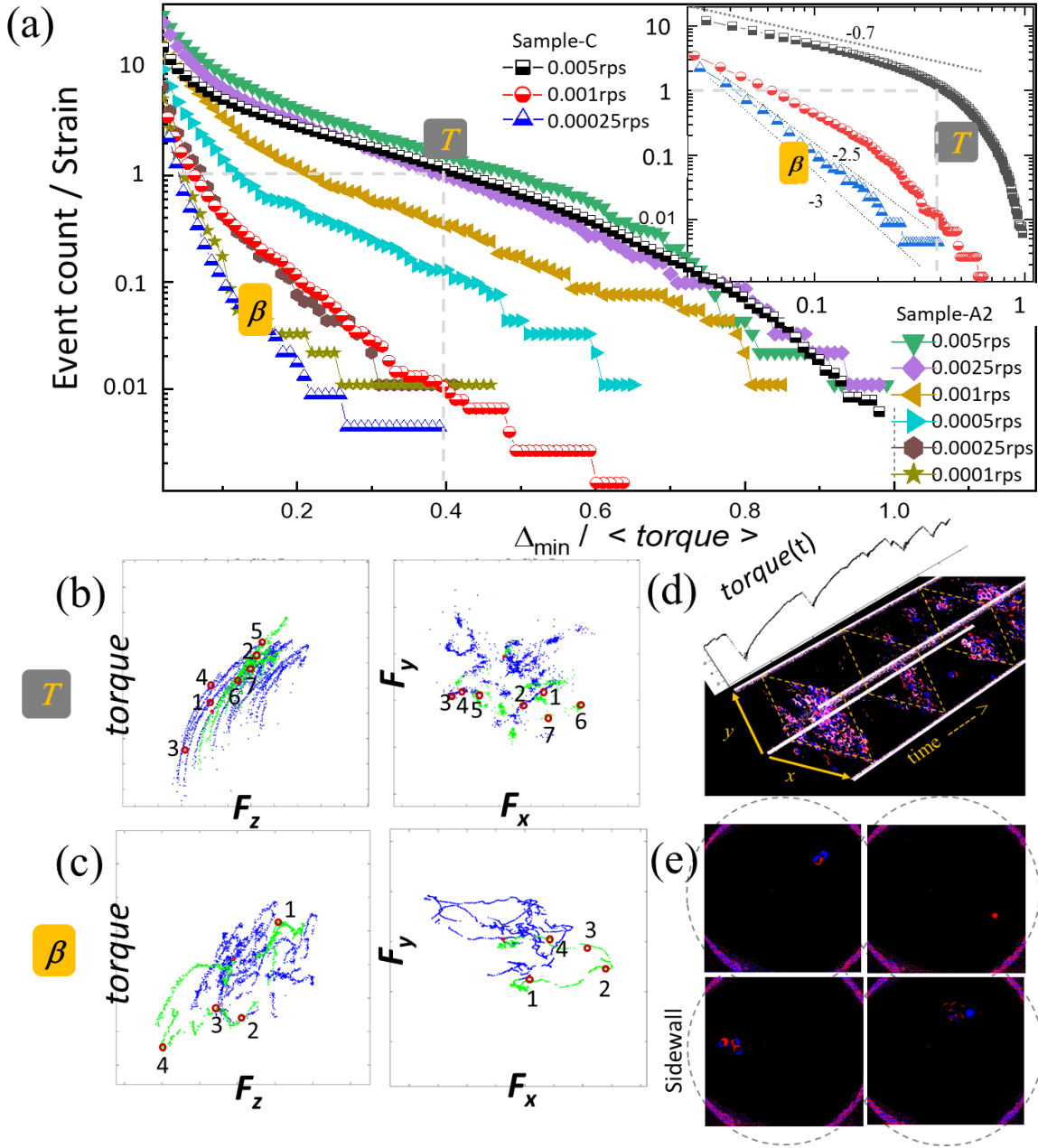


FIG.2 (a) Cumulative distribution of drop events with $|\Delta \text{torque}| > \Delta_{\min}$, for experiments at different driving rates indicated in rps. Event counts are normalized by the strain accumulated. Data include experiments using two batches of particles (A2 and C) in the same fluid. $\phi=0.56$. **(b-c)** Scattered plots of $\{\text{torque vs. } F_z\}$ simultaneously with $\{F_y \text{ vs. } F_x\}$, for state-T and state- β , respectively. Numbers represent time-ordered sequence; these graphs are also presented in animations online. Each axis spans $\pm 2\text{RMS}$ of the variable it represents around its mean value. Data are accumulated with a total angular rotation of 0.3, in which an interval corresponding to *unit strain* is marked in green. Animated versions are provided online[33]. **(d)** Stacked sequence of δf in-sync with $\text{torque}(t)$, for state-T, with $\delta\theta=2\pi\cdot 10^{-4}$. **(e)** Four typical frames of δf with $\delta\theta=2\pi\cdot 10^{-4}$, for state- β .

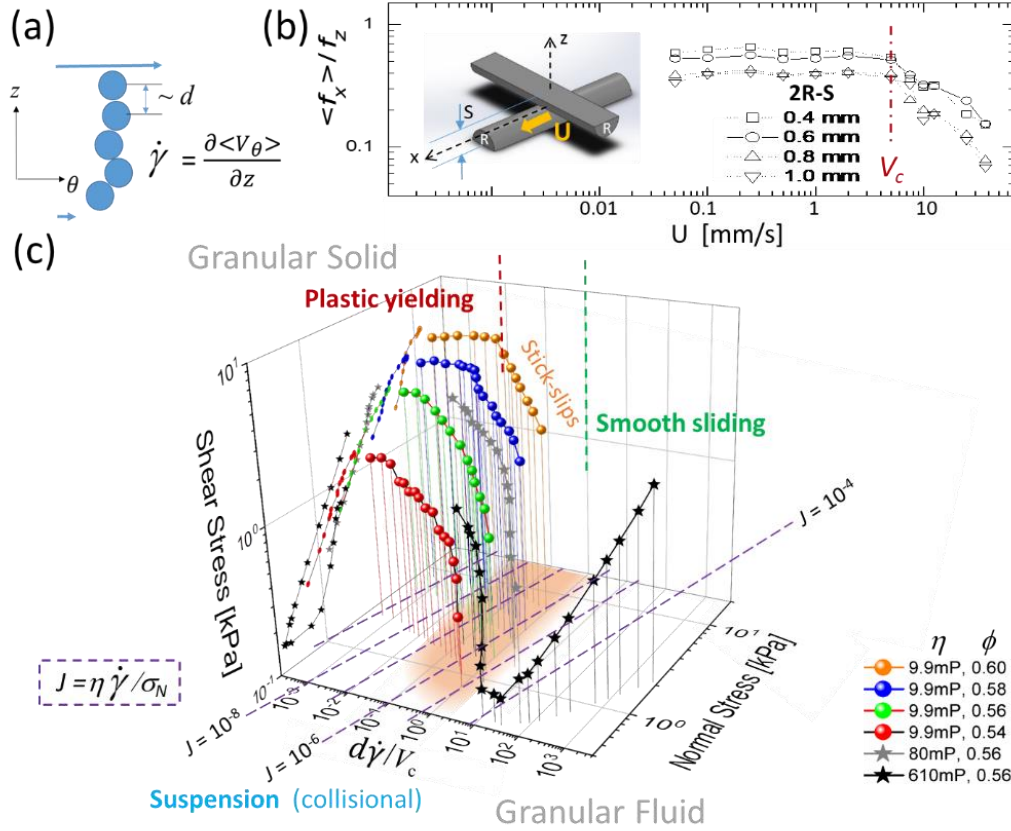


FIG.3 (a) Illustration of the motion of densely packed particles under an imposed shear rate $\dot{\gamma}$; (b) Schematics and results of measurements on the average tangential force f_x , normalized by the normal force f_z , for a localized contact between PDMS surfaces with a radius of curvature R . Data are plotted as functions of the sliding speed, for experiments at multiple pressing depths (controlled by the distance S between the base planes) up to about $0.1d$. Data reveals a critical velocity V_c that appears insensitive to the pressing depth. (c) Proposed phase diagram presented with data from experiments with different values of ϕ and η . The 3D plot consists of the time-averaged shear stress σ_s as the vertical coordinate, plotted against the dimensionless shear rate $d\dot{\gamma}/V_c$ and normal stress σ_N . Contours of $J = 10^{-4}$ down to 10^{-9} are displayed by dashed lines.

- [1] É. Guazzelli and O. Pouliquen, Rheology of Dense Granular Suspensions, *J. Fluid Mech.* **852**, P1 (2018).
- [2] A. Nicolas, E. E. Ferrero, K. Martens, and J.-L. Barrat, Deformation and Flow of Amorphous Solids: Insights from Elastoplastic Models *Rev. Mod. Phys.* **90**, 045006 (2018).
- [3] I. S. Aranson, L. S. Tsimring, F. Malloggi, and E. Clément, Nonlocal Rheological Properties of Granular Flows near a Jamming Limit, *Phys. Rev. E* **78**, 031303 (2008).
- [4] D. L. Henann and K. Kamrin, Size-Dependent Continuum Model for Dense Granular Flows, *Proc. Natl. Acad. Sci.* **110**, 6730 (2013).
- [5] K.-L. Lee and F.-L. Yang, Relaxation-Type Nonlocal Inertial-Number Rheology for Dry Granular Flows, *Phys. Rev. E* **96**, 062909 (2017).
- [6] D. Bonn, M. M. Denn, L. Berthier, T. Divoux, and S. Manneville, Yield Stress Materials in Soft Condensed Matter, *Rev. Mod. Phys.* **89**, 035005 (2017).
- [7] A. J. Liu and S. R. Nagel, Jamming Is Not Just Cool Any More, *Nature* **396**, 21 (1998).
- [8] L. E. Silbert, Jamming of frictional spheres and random loose packing, *Soft Matter* **6**, 2918 (2010).
- [9] D. Bi, J. Zhang, B. Chakraborty, and R. P. Behringer, Jamming by Shear, *Nature* **480**, 355 (2011).
- [10] T. Shen, C. S. O'Hern, and M. D. Shattuck, Contact Percolation Transition in Athermal Particulate Systems, *Phys. Rev. E* **85**, 011308 (2012).
- [11] M. M. Bandi, M. K. Rivera, F. Krzakala, and R. E. Ecke, Fragility and Hysteretic Creep in Frictional Granular Jamming, *Phys. Rev. E* **87**, 042205 (2013).
- [12] J. R. Royer and P. M. Chaikin, Precisely Cyclic Sand: Self-Organization of Periodically Sheared Frictional Grains, *Proc. Natl. Acad. Sci.* **112**, 49 (2015).
- [13] E. Brown, N. A. Forman, C. S. Orellana, H. Zhang, B. W. Maynor, D. E. Betts, J. M. DeSimone, and H. M. Jaeger, Generality of Shear Thickening in Dense Suspensions, *Nat. Mater.* **9**, 220 (2010).
- [14] N. Fernandez, R. Mani, D. Rinaldi, D. Kadau, M. Mosquet, H. Lombois-Burger, J. Cayer-Barrioz, H. J. Herrmann, N. D. Spencer, and L. Isa, Microscopic Mechanism for Shear Thickening of Non-Brownian Suspensions, *Phys. Rev. Lett.* **111**, 108301 (2013).
- [15] C. Clavaud, A. Bérut, B. Metzger, and Y. Forterre, Revealing the Frictional Transition in Shear-Thickening Suspensions, *Proc. Natl. Acad. Sci.* **114**, 5147 (2017).
- [16] R. Mari, R. Seto, J. F. Morris, and M. M. Denn, Shear Thickening, Frictionless and Frictional Rheologies in Non-Brownian Suspensions, *J. Rheol.* **58**, 1693 (2014).
- [17] S. Jamali and J. F. Brady, Alternative Frictional Model for Discontinuous Shear Thickening of Dense Suspensions: Hydrodynamics, *Phys. Rev. Lett.* **123**, 138002 (2019).
- [18] C. H. Scholz, *Nature* **391**, Earthquakes and Friction Laws, 37 (1998).
- [19] E. A. Jagla, F. P. Landes, and A. Rosso, Viscoelastic Effects in Avalanche Dynamics: A Key to Earthquake Statistics, *Phys Rev Lett* **112**, 174301 (2014).
- [20] S. Ide, G. C. Beroza, D. R. Shelly, and T. Uchide, A Scaling Law for Slow Earthquakes, *Nature* **447**, 76 (2007).
- [21] H. Perrin, C. Clavaud, M. Wyart, B. Metzger, and Y. Forterre, , Interparticle Friction Leads to Nonmonotonic Flow Curves and Hysteresis in Viscous Suspensions, *Phys Rev X* **9**, 031027 (2019).
- [22] M. Workamp and J. A. Dijksman, , Contact Tribology Also Affects the Slow Flow Behavior of Granular Emulsions, *J. Rheol.* **63**, 275 (2019).
- [23] J.-C. Tsai, G. A. Voth, and J. P. Gollub, *Phys. Rev. Lett.* **91**, 064301 (2003).
- [24] J. A. Dijksman, F. Rietz, K. A. Lőrincz, M. van Hecke, and W. Losert, *Rev. Sci. Instrum.* **83**, 011301 (2012).
- [25] The Dow Chemical, Sylgard-184
- [26] D. Lootens, H. Van Damme, and P. Hébraud, Giant Stress Fluctuations at the Jamming Transition, *Phys. Rev. Lett.* **90**, 178301 (2003).
- [27] V. Rathee, D. L. Blair, and J. S. Urbach, Localized Stress Fluctuations Drive Shear Thickening in Dense Suspensions, *Proc. Natl. Acad. Sci.* **114**, 8740 (2017).
- [28] J. F. Morris, Shear Thickening of Concentrated Suspensions: Recent Developments and Relation to Other Phenomena, *Annu. Rev. Fluid Mech.* **52**, (2020).
- [29] *Dynamical Heterogeneities in Glasses, Colloids, and Granular Media* (Oxford University Press, 2011).
- [30] J. H. H. Bongaerts, K. Fourtouni, and J. R. Stokes, Soft-Tribology: Lubrication in a Compliant PDMS–PDMS Contact, *Tribol. Int.* **40**, 1531 (2007).
- [31] F. Boyer, É. Guazzelli, and O. Pouliquen, Unifying Suspension and Granular Rheology, *Phys. Rev. Lett.* **107**, 188301 (2011).
- [32] E. DeGiuli and M. Wyart, Friction Law and Hysteresis in Granular Materials, *Proc. Natl. Acad. Sci.* **114**, 9284 (2017).
- [33] <http://www.phys.sinica.edu.tw/jctsai/brittle/>